CHEMISTRY OF MATERIALS

ARTICLE

pubs.acs.org/cm

Large-Scale Synthesis of Ultrathin Manganese Oxide Nanoplates and Their Applications to T1 MRI Contrast Agents

Mihyun Park,[†,‡] Nohyun Lee,[†,‡] Seung Hong Choi,[§] Kwangjin An,[†,‡] Seung-Ho Yu,[‡] Jeong Hyun Kim,[†,‡] Seung-Hae Kwon,[⊥] Dokyoon Kim,[†,‡] Hyoungsu Kim,[§] Sung-Il Baek,[∥] Tae-Young Ahn,[∥] Ok Kyu Park,[⊥] Jae Sung Son,[†,‡] Yung-Eun Sung,[‡] Young-Woon Kim,[∥] Zhongwu Wang,[#] Nicola Pinna,[‡,▽] and Taeghwan Hyeon*[,†,‡]

[†]National Creative Research Initiative Center for Oxide Nanocrystalline Materials, and School of Chemical and Biological Engineering, Seoul National University, Seoul 151-744, Korea

[‡]World Class University (WCU) Program of Chemical Convergence for Energy & Environment (C2E2), and School of Chemical and Biological Engineering, Seoul National University, Seoul 151-744, Korea

[§]Diagnostic Radiology, Seoul National University Hospital, and Institute of Radiation Medicine, Medical Research Center, Seoul National University, Seoul 110-744, Korea

[∥]School of Materials Science & Engineering, Seoul National University, Seoul 151-744, Korea

[⊥]Korea Basic Science Institute, Chuncheon 200−701, Korea

[#]Cornell High Energy Synchrotron Source and Wilson Laboratory, Cornell University, Ithaca, New York 14853, United States

[▽]Department of Chemistry and CICECO, University of Aveiro, 3810-193 Aveiro, Portugal

Supporting Information

ABSTRACT: Lamellar structured ultrathin manganese oxide nanoplates have been synthesized from thermal decomposition of manganese(II) acetylacetonate in the presence of 2,3-dihydroxynaphthalene, which promoted two-dimensional (2-D) growth by acting not only as a strongly binding surfactant but also as a structure-directing agent. Ultrathin manganese oxide nanoplates with a thickness of about 1 nm were assembled into a lamellar structure, and the width of the nanoplates could be controlled from 8 to 70 nm by using various coordinating solvents. X-ray absorption near-edge structure (XANES) spectra at the Mn K edge clearly showed that the nanoplates are mainly composed of Mn(II) species with octahedral symmetry. These hydrophobic manganese oxide nanoplates were ligand-exchanged with amine-terminated poly(ethyleneglycol) to generate water-dispersible nanoplates and applied to T1 contrast agents for magnetic resonance imaging (MRI). They exhibited a very high longitudinal relaxivity (r_1) value of up to 5.5 $mM^{-1}s^{-1}$ derived from their high concentration of manganese ions exposed on the surface, and strong contrast enhancement of *in vitro* and *in vivo* MR images was observed with a very low dose.

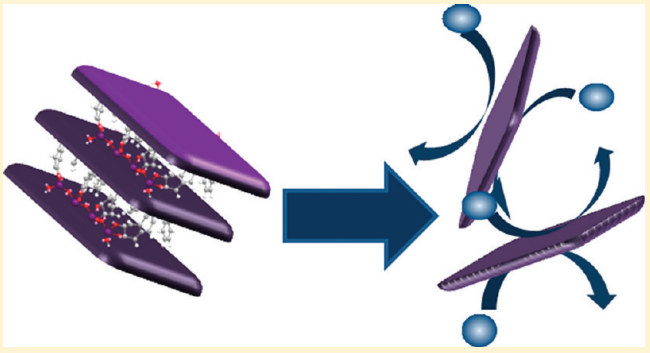

KEYWORDS: manganese oxide, nanoplates, $\pi-\pi$ interactions, magnetic resonance imaging, contrast agent

INTRODUCTION

Nanoplates and related two-dimensional (2-D) nanostructured materials have attracted tremendous attention from many researchers in various disciplines for their unique properties.[1−13] Thin 2-D nanomaterials have many potential applications in catalysis, solar cells, and electrochemical devices as a result of their high surface areas, which provide enhanced interfacial interactions. There have been several reports on the synthesis of thin 2-D nanomaterials with a uniform thickness of <2 nm.[14−23] Several groups have synthesized nanosheets of metal chalcogenides with thicknesses of 1−2 nm via the reaction of metal precursors with chalcogenide reagents.[14−18] Various oxide nanocrystals of sub-2 nm thickness were synthesized using colloidal synthetic methods.[19] However, colloidal synthesis of ultrathin 2-D transition metal oxide nanostructures with thicknesses of less than 1 nm has been rarely reported.[20−23]

Surfactants, which are extensively utilized for the colloidal synthesis of nanocrystals, are sometimes used as structure-directing agents for the synthesis of ultrathin 2-D nanostructured materials.[24−29] Consequently, it is very important to choose

Received: February 9, 2011
Revised: June 10, 2011
Published: June 30, 2011

appropriate surfactants that are able to induce confined crystal growth. In general, strongly binding surfactants inhibit crystal growth, resulting in small-sized nanoparticles.[30−32] For example, surfactants with bidentate enediol groups such as dopamine and catechol have been used to synthesize iron oxide nanoparticles of <2.5 nm.[33] Consequently, careful selection of surfactants having both strong binding moieties and structure-directing capabilities is critical for the synthesis of ultrathin 2-D nanoplates. Herein, we report on the synthesis of manganese oxide nanoplates with sub-nanometer thickness from thermal decomposition of manganese(II) acetylacetonate in the presence of 2,3-dihydroxynaphthalene (2,3-DHN), which promoted 2-D growth by acting not only as a strongly binding surfactant but also as a structure-directing agent. In other words, strong binding of the bidentate enediol ligand of 2,3-DHN to the various surfaces[34−40] and the $\pi-\pi$ interaction regulating the self-assembly of naphthalene rings[41−43] have seemingly led to the formation of ultrathin nanoplates. Furthermore, the synthesized ultrathin nanoplates were successfully applied as a magnetic resonance imaging (MRI) contrast agent with an extremely high relaxivity due to their high surface-to-volume ratio.

EXPERIMENTAL SECTION

Chemicals. Manganese(II) acetylacetonate ($Mn(acac)_2$, 98%), 2,3-dihydroxynaphthalene (2,3-DHN, 90%), and benzyl ether (99%) were purchased from Aldrich Chemical Co. Iron(III) acetylacetonate ($Fe(acac)_3$, 99%) and oleylamine (80−90%) was purchased from Acros Organics.

Synthesis of 8 nm-Sized MnO_x Nanoplates. Synthesis was carried out under an argon atmosphere using standard Schlenk line techniques. In a typical synthesis, 2 mmol of $Mn(acac)_2$ (0.506 g) was added to a mixture containing 4 mmol of 2,3-DHN (0.640 g) and 10 g of benzyl ether. The mixture solution was degassed at room temperature for 1 h. The solution was then heated to 300 °C at a heating rate of 10 °C min^{-1} and was maintained at this temperature for 10 min. After cooling the solution to room temperature, a mixture of 10 mL of chloroform and 50 mL of methyl alcohol was added to the solution. The solution was then centrifuged at 1700 rpm for 10 min to precipitate the nanoplates. The separated nanoplates were washed using 20 mL of chloroform and 50 mL of methyl alcohol.

Synthesis of 20 nm-Sized MnO_x Nanoplates. Two millimoles of $Mn(acac)_2$ (0.506 g) was added to a mixture containing 4 mmol of 2,3-DHN (0.640 g) and 10 g of oleylamine. The mixture solution was degassed at room temperature for 1 h. The solution was then heated to 300 °C at a heating rate of 10 °C min^{-1} and was maintained at this temperature for 30 min. The rest of the procedures are the same as those described above.

Synthesis of FeOx Nanoplates. Two millimoles of $Fe(acac)_3$ (0.706 g) was added to a mixture composed of 4 mmol of 2,3-DHN (0.640 g) and 10 g of oleylamine. The mixture solution was degassed at room temperature for 1 h. The solution was then heated to 300 °C at a heating rate of 10 °C min^{-1} and was maintained at this temperature for 5 min. The rest of the procedures are the same as those described above.

Ligand Exchange. Twenty milligrams of the nanoplates and 80 mg of amine-terminated polyethylene glycol (NH_2-PEG; M_w. 2000) were mixed in 30 mL of $CHCl_3$, and then the solvent was removed by evaporation and finally kept under vacuum at 120 °C for 1 h. The addition of water resulted in the production of a dark brown suspension. The residual organic compound was removed by two cycles of filtration and ultracentrifugation at 40000 rpm for 4 h. To investigate the possibility of leaching of the Mn(II) ion from the nanoplates, Mn(II) ion concentrations of the solutions before and after ultracentrifugation were measured by inductively coupled plasma atomic emission spectroscopy (ICP-AES).

Dye Conjugation. For dye conjugation, 20 mg of nanoplates was ligand-exchanged with 60 mg of NH_2-PEG and 20 mg of $NH_2-PEG-NH_2$ (M_w 2000) using a procedure similar to that described above. The resulting ligand-exchanged nanoplates were dispersed in 2 mL of carbonate buffer (100 mM, pH 9.5), and 0.2 mg of rhodamine-B-isothiocyanate (RITC) dissolved in 100 μL DMSO was added to the nanoplate solution. After 2 h of incubation, free RITC was removed using a PD-10 desalting column by washing with phosphate buffered saline (100 mM, pH 7.4).

Characterization. The synthesized nanoplates were characterized by transmission electron microscopy (TEM), scanning transmission electron microscopy (STEM), X-ray diffraction (XRD), X-ray photoelectron spectroscopy (XPS), and atomic force microscopy (AFM). TEM and STEM images were obtained with JEOL 2010 and FEI Tecnai F-20 microscopy operated at 200 kV. Powder X-ray diffraction patterns were obtained with a Rigaku D/Max-3C diffractometer equipped with a rotating anode and a Cu Kα radiation source (λ = 0.15418 nm). The Mn K-edge X-ray absorption spectra were recorded on the 10A beamline at the Pohang Light Source (PLS). The optical properties were characterized by using a JASCO V-550 UV−vis spectrophotometer.

Synchrotron-radiation X-ray diffraction measurements were performed at the B2 station of Cornell High Energy Synchrotron Source at Cornell University. The monochromatic synchrotron X-ray beam was optimized at an energy of 25 keV, equivalent to the wavelength of 0.486 Å. The original 1 mm X-ray beam was collimated into a smaller size of 100 μm. Upon shooting of the X-ray beam on the samples, a series of two-dimensional X-ray diffraction images were collected by a large area MAR345 detector. The detector had a total pixel number of 3450 × 3450 (vertical vs horizontal) in which the single pixel size is 100 μm. The distance between the sample and detector was calibrated by a standard CeO_2 powder.

Cell Viability. The viability in the presence of nanoplates was evaluated using the 3-[4,5-dimethylthialzol-2-yl]-2,5-diphenyltetrazolium bromide (MTT, Sigma) assay. MCF-7 cells, which are human breast cancer cells, were seeded into 96-well plates at a density of 1×10^4 per well in 200 μL of media and grown overnight. The cells were then incubated with various concentrations of the nanoplates (0, 1.56, 3.13, 6.25, 12.5, 25, 50, and 100 μg Mn mL^{-1}) for 24 h. Following this incubation, cells were incubated in media containing 0.1 mg/mL of MTT for 1 h. Thereafter, the MTT solution was removed, and the precipitated violet crystals were dissolved in 200 μL of DMSO. The absorbance was measured at 560 nm using a VersaMax microplate reader (Molecular Devices).

Measurement of MRI Properties of the Nanoplates. A 1.5 T clinical MRI scanner was used to measure the T1 and T2 relaxation times for various concentrations of the nanoplates dispersed in water. (Mn concentration was measured by inductively coupled plasma atomic emission spectroscopy (ICP-AES).) An IR-FSE sequence with 30 different values of TI (TR/TE/TI = 4400 ms/13 ms/24−4000 ms) for T1 measurements and a conventional CPMG sequence with 12 different TE values (TR/TE = 3300 ms/13, 26, 39, 52, 70, 140, 210, 280, 400, 800, 1200, and 1600 ms) for T2 measurements were performed with a head coil on the 1.5 T MRI scanner. T1 and T2 relaxation times were calculated by fitting the signal intensities with increasing TE or TI to a monoexponential function or $|[1 - (1 - k)\cdot\exp(-TI/T1)]\cdot Mo|$ by using a nonlinear least-squares fit of the Levenberg−Marquardt algorithm.

To prepare the *in vitro* MR phantom, MCF-7 cells were seeded onto culture dishes at a density of 1×10^6 per plate in 10 mL of media and grown overnight. Following this, nanoplates of various concentrations (0−100 μg Mn mL^{-1}) were added. After 24 h, the cells were washed twice in PBS to remove free nanoplates and then detached by the addition of 1 mL of trypsin/EDTA. After centrifugation at 1500 rpm for

5 min, cells were dispersed in 2 mL of culture media and transferred to a 1.5 mL microtube. Cell pellets were prepared by centrifugation at 2000 rpm for 5 min. The measurement parameters are as follows: flip angle = 73, ETL = 1, TR = 500 ms, TE = 10 ms, field of view FOV = 120 × 120 mm^2, matrix = 256 × 256, slice thickness/gap = 2 mm/2 mm, and NEX = 2.0

In vivo MR images were obtained by the following procedure. The *in vivo* experiments were approved by the Institutional Animal Care and Use Committee (IACUC) of the Clinical Research Institute of Seoul National University Hospital. Mice (avg. weight 25 g) were imaged using a wrist coil on a 1.5 T MRI scanner. After the acquisition of preinjection images, an appropriate dose of the nanoplates was intravenously injected via tail vein. The animal images were acquired up to a week. The measurement parameters are as follows: flip angle = 15, ETL = 1, TR = 5.8 ms, TE = 22.1 ms, field of view FOV = 80 × 80 mm^2, matrix = 256 × 256, slice thickness/gap = 1.4 mm/1.4 mm, and NEX = 2.0.

Tissue Imaging. Mice were sacrificed after intravenous injection of RITC conjugated nanoplates. The liver was harvested, fixed with 4% formaldehyde, and embedded in paraffin. The tissues were sectioned and mounted on slide glasses. The slides were counterstained with DAPI. Fluorescence images were acquired by confocal laser scanning microscopy.

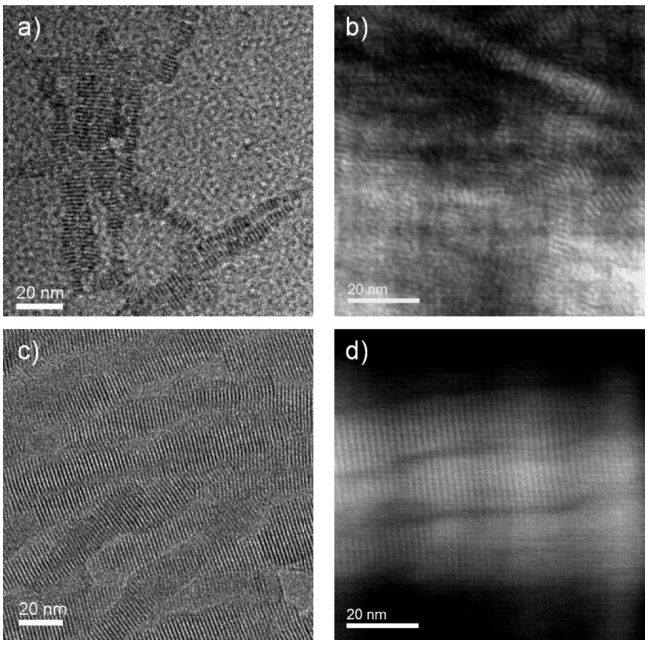

Figure 1. TEM (a,c) and STEM (b,d) images of the lamellar structured manganese oxide nanoplates with widths of 8 nm (a,b) and 20 nm (c,d).

RESULTS AND DISCUSSION

Transmission electron microscopic (TEM) and scanning transmission electron microscopic (STEM) images show that ultrathin manganese oxide nanoplates with thicknesses of about 1 nm were assembled into a lamellar structure (Figure 1). The width of the nanoplates was controlled by changing the solvents (Figure 1 and Figure S1, Supporting Information). The width of the nanoplates synthesized using benzyl ether was smaller (~ 8 nm, Figure 1a and b) than that of the nanoplates produced using oleylamine (~20 nm, Figure 1c and d). It was possible to prepare the nanoplates of widths up to ~70 nm using octyl ether as a solvent (Figure S1, Supporting Information). In the case of various ether solvents, the mean width of the nanoplates decreased as the solubility of 2,3-DHN in ether increased. Aromatic ether seems to enhance the solubility of 2,3-DHN through $\pi-\pi$ interaction. Therefore, employing an alkyl ether (e.g., octyl ether) as solvent resulted in aggregation of 2,3-DHN, and nanoplates with large widths were produced. The presence of highly ordered lamellar structures implies that 2,3-DHN molecules on the neighboring nanoplates are interdigitated. The detailed arrangement of the intercalating 2,3-DHN molecules was investigated by UV−vis absorption spectroscopy. Stacked aromatic rings exhibit distinct changes in the absorption band compared to the free-standing monomeric species.[42,44−46] Two possible arrangements of the aromatic rings, head-to-tail (J-aggregation, stabilized) and head-to-head (H-aggregation, destabilized), are distinguished by red- and blue-shifts of the absorption peak in the UV−vis spectra, respectively. The observed absorption spectrum of the assembled nanoplates was broader and red-shifted compared to that of monomeric 2,3-DHN, suggesting that 2,3-DHN molecules on the adjacent nanoplates are in a head-to-tail arrangement (Figure 2).

The lamellar structure of the assembled nanoplates was further characterized by small-angle X-ray diffraction (SAXRD) using a synchrotron radiation source. In Figure 3, the SAXRD data clearly demonstrate the lamellar ordering of the nanoplates. The peak at $2\theta = 1.6°$ indicates an interplate distance of 1.8 nm. Considering that the molecular dimension of a naphthalene ring is about 0.89 Å[45] and that neighboring naphthalene rings are in a head-to-tail arrangement, the estimated thickness of the nanoplates is less than 1 nm. The estimated thickness is well-matched

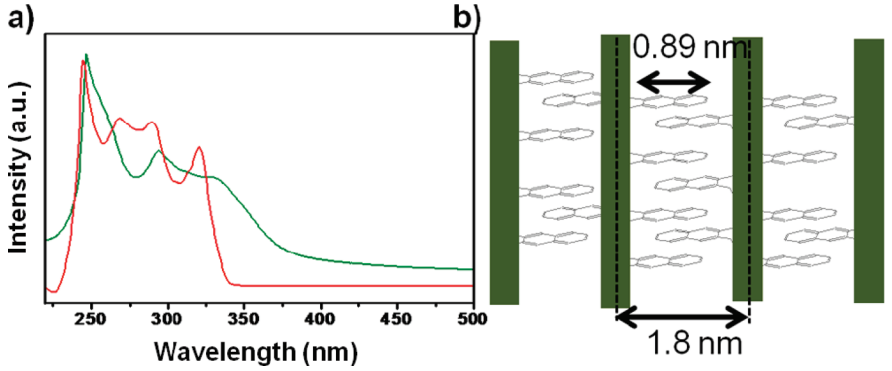

Figure 2. (a) UV−vis absorption spectra of free 2,3-DHN (red) and manganese oxide nanoplates (green). (b) Schematic diagram of J- aggregated nanoplates.

dx.doi.org/10.1021/cm200414c |*Chem. Mater.* 2011, 23, 3318–3324

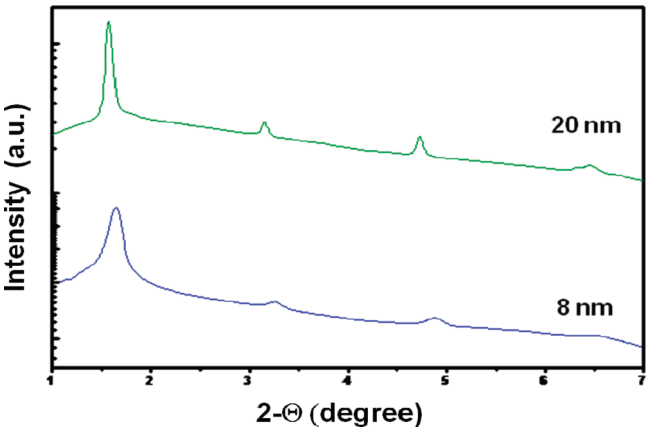

Figure 3. Small angle X-ray diffraction patterns of 8 and 20 nm-sized manganese oxide nanoplates.

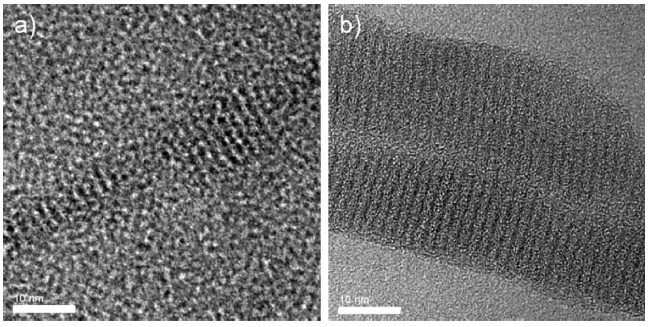

Figure 4. High resolution TEM images of the nanoplates with widths of (a) 8 nm and (b) 20 nm.

with observed thickness in high resolution TEM (HRTEM) images (Figure 4). The HRTEM images demonstrated that the strong binding ability of 2,3-DHN inhibited growth along the thickness direction, resulting in nanoplates with subnanometer thickness. The current synthetic process is easy to scale up, and when we ran the reaction using 20 mmol of manganese precursor, 3.8 g of manganese oxide nanoplates were obtained in a single batch (Figure S2, Supporting Information). Furthermore, lamellar-structured iron oxide nanoplates were produced by a similar synthetic process (Experimental Section and Figure S3, Supporting Information), demonstrating that the current synthetic method can be extended to other metal oxide nanoplates. Interestingly, the interlamellar spacing extracted from the SAXRD data of the iron oxide nanoplates was comparable to that of manganese oxide nanoplates.

X-ray absorption near-edge structure (XANES) at the Mn K edge was employed to elucidate the manganese oxidation state of the nanoplates.[48] The Mn K-edge XANES spectra of the nanoplates and various standard manganese oxides are shown in Figure 5. As the oxidation state increased, the main edge peak shifted to a higher energy. These XANES spectra clearly showed that the nanoplates are mainly composed of Mn(II) species. Furthermore, the small absorption at the pre-edge region indicated the octahedral symmetry of Mn ions in the nanoplates. The wide angle XRD pattern of the 20 nm nanoplates using a synchrotron radiation source is highly complicated because the peaks from the lamellar structure overlap with those from the

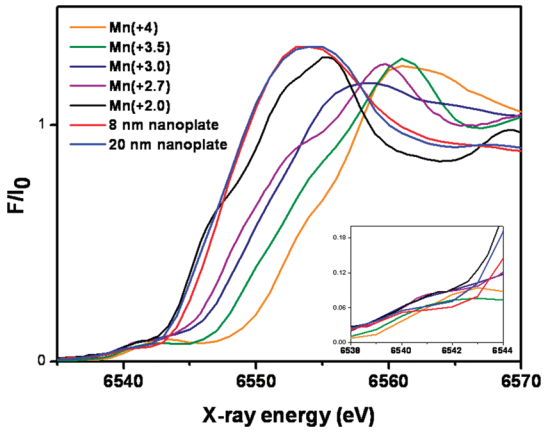

Figure 5. XANES spectra of 8 nm- and 20 nm-sized manganese oxide nanoplates, and various standard manganese oxide samples (from the bottom, MnO, Mn_3O_4, Mn_2O_3, $LiMn_2O_4$, and MnO_2). The inset is the pre-edge region of the spectra.

crystal structure of the individual nanoplates (Figure S4, Supporting Information). Moreover, surface reconstruction resulting from huge compressive stress exerted on the subnanometer thick nanoplates can dramatically modify the XRD pattern.[49,14] To characterize the crystal structure, the nanoplates were annealed under Ar atmosphere at 500 °C, and the resulting XRD pattern matched very well with the MnO structure. Furthermore, when both 8 nm-sized nanoplates and 5 nm-sized spherical MnO nanoparticles were oxidized at 400 and 500 °C under air, both nanostructured materials were transformed into Mn_3O_4 or Mn_2O_3 (Figure S5, Supporting Information). From the XANES and XRD data after thermal treatments, we propose that the nanoplates have a modified MnO crystal structure.

To evaluate the performances of the nanoplates as an MRI contrast agent, the nanoplates were dispersed in water by ligand exchange with amine-terminated polyethylene glycol (NH_2—PEG). The resulting aqueous dispersion containing the nanoplates was nearly transparent, suggesting that most of the 2,3-DHN was removed and that the lamellar structure was delaminated to form well-dispersed nanoplates.[50] The STEM image showed that the nanoplates were well-dispersed on a TEM grid (Figure 6a). UV—vis absorption spectra showed a significant decrease of the absorption peak of 2,3-DHN, demonstrating that most of the 2,3-DHN was removed during the ligand-exchange reaction (Figure 6b). Dynamic light scattering results revealed that the hydrodynamic diameter of the 8 nm-sized nanoplates was only 23 nm (Figure S6, Supporting Information). To investigate the potential leaching of manganese ions, we compared the manganese concentration of the supernatant solutions after keeping for 1 day and 7 days in the presence of nanoplates and subsequently ultracentrifuging. A very similar and small amount of manganese ion was detected in the supernatant solutions after keeping at room temperature for 1 day and 7 days (Table S1, Supporting Information). We presume that the detected small amount of manganese ion resulted from the diffusion of the nanoplates to the supernatant solution after ultracentrifugation (Figure S7, Supporting Information) and that nearly no manganese ion was leached.

MR relaxivity was measured with a 1.5 T clinical MR scanner. The 8 and 20 nm-sized nanoplates were found to have longitudinal relaxivity (r_1) values of 5.5 and 2.13 mM^{-1} s^{-1}, and

dx.doi.org/10.1021/cm200414c |*Chem. Mater.* 2011, 23, 3318–3324

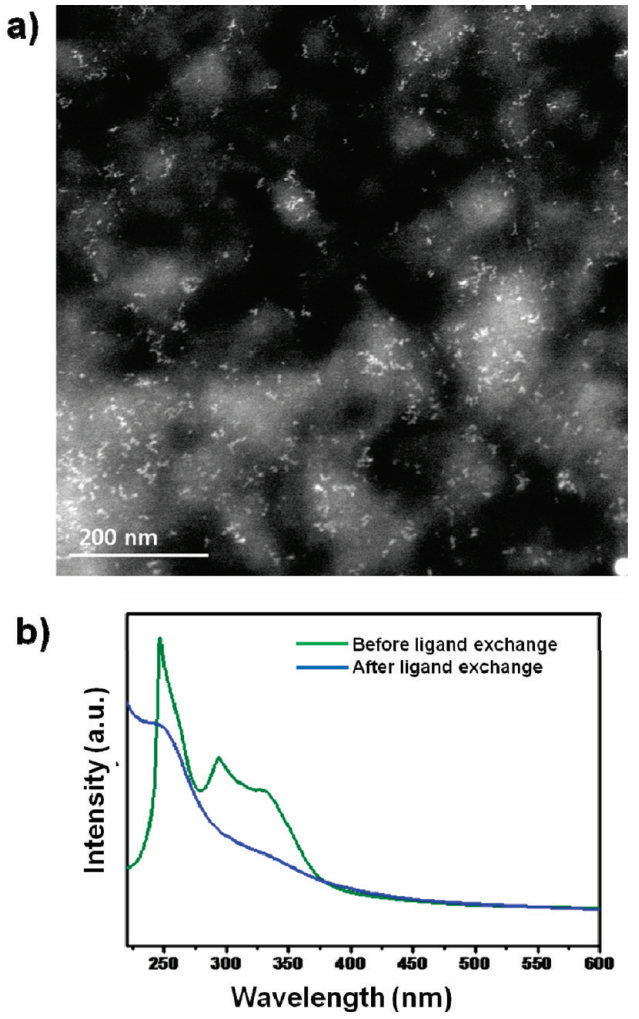

Figure 6. Eight nanometer-sized nanoplates after the ligand exchange process. (a) STEM image of water dispersed nanoplates. (b) UV−vis absorption spectra of the nanoplates before (green) and after ligand exchange (blue).

transverse relaxivity (r_2) values of 9.86 and 4.31 mM^{-1} s^{-1} (on the basis of the Mn ion concentration), respectively. There were several efforts to increase r_1 of nanoparticle-based MRI contrast agents, including synthesis of hollow nanoparticles or nanostructured metal−organic frameworks.[41−58] The observed r_1 values of the nanoplates are among the highest compared to those of previously reported manganese oxide nanoparticle-based MRI contrast agents (Table 1). To examine the correlation between the surface to volume ratios and longitudinal relaxivity values, we used the Pearson product moment correlation. It is calculated by dividing the covariance of the two variables by the product of their standard deviations. The Pearson coefficient, calculated from a set of manganese oxide nanoparticles, was 0.93, indicating a strong correlation between the surface area and the longitudinal relaxivity value. A large number of paramagnetic manganese ions exposed on the surface accelerate the spin relaxation process of water protons and consequently shorten the T1 relaxation time.[59]

In vitro and *in vivo* MR imaging experiments were performed using the 8 nm-sized nanoplates. Before MR imaging, the cytotoxic effect of the nanoplates on MCF-7 cells was measured

Table 1. Relaxivity Comparisons of Various MnO-Based Nanostructured Materials

material		S/V	r_1	r_2
MnO nanoplate	8 nm	2.92	5.5	9.86
	20 nm	2.1	2.13	4.31
MnO spherical nanoparticle[55]	3 nm	2	2.38	7.27
	5 nm	1.2	1.39	3.66
	11 nm	0.55	0.99	2.84
	13 nm	0.46	0.41	1.26
MnO hollow nanoparticle[56]	20 nm spherical nanoparticles	0.3	0.35	8.68
	20 nm hollow nanoparticles	0.68	1.15	6.737
Pearson correlation coefficient between S/V and r_1		**0.93**		

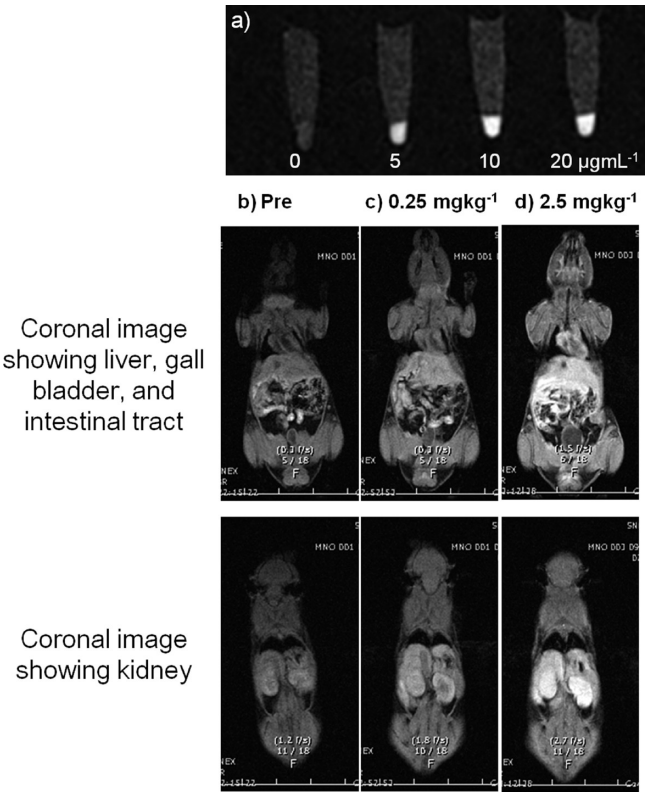

Figure 7. *In vitro* and *in vivo* T1-weighted MR images. (a) *In vitro* MR images of MCF-7 cells incubated with various concentrations of 8 nm nanoplates. *In vivo* MR images of a mouse (b) before injection, immediately after the injection of the nanoplates at (c) 0.25 mg kg^{-1} and (d) 2.5 mg kg^{-1} Mn dose.

by the 3-(4,5-dimethylthiazol-2-yl)-2,5-diphenyltetra-zolium bromide (MTT) assay for the determination of adequate dose level (Figure S8, Supporting Information). The MTT assay result showed that the manganese oxide nanoplates are toxic to cells at a manganese concentration of over 25 μg mL^{-1}. Figure 7a shows the *in vitro* cellular MR images acquired after incubation with 5, 10, and 20 μg mL^{-1} of the nanoplates for 24 h. Even with a very small dose, a discernible difference between the brightness levels of control cells and cells incubated with the nanoplates was observed, and the brightness was enhanced as the manganese ion

dx.doi.org/10.1021/cm200414c |*Chem. Mater.* 2011, 23, 3318–3324

concentration increased. The ability to obtain a bright image with a low dose of contrast agent is strongly desirable for *in vivo* MRI applications. To test the feasibility of the nanoplates as an MR contrast agent, an *in vivo* MR study was performed on mice. Coronal MR images (Figure 7b−d) were acquired after intravenous injection of the nanoplates. The contrast of blood vessels and entire organs including the brain rapidly increased. This MR contrast enhancement effect could be readily observed for the whole body image even with an injection of 0.25 mg of Mn (measured by ICP-AES) per kg of mouse body weight. Biodistribution of the injected nanoplates was investigated for up to one week (Figure S9, Supporting Information). Upon entering the bloodstream, the nanoplates were distributed throughout the entire body, including the liver, gall bladder, and kidney. The MR signal of the liver and spleen was enhanced immediately after the injection of the nanoplates due to the rapid uptake by the reticuloendothelial system (RES). After a while, the gall bladder was enhanced since the bile duct was in the route of excretion of hepatocytes. It was estimated that the nanoplates were taken up not only by the Kupffer cell, which is the representative cell of the RES, but also by the hepatocytes. Hepatic uptake of the nanoplates was demonstrated by a confocal laser scanning microscopy image of the liver cells after the intravenous injection of RITC conjugated nanoplates (Figure S10, Supporting Information).[60−62] Finally, after a week, the brightness of the MR images dropped dramatically to that of the preinjection model.

CONCLUSIONS

In conclusion, ultrathin manganese oxide nanoplates were synthesized via thermal decomposition of manganese(II) acetylacetonate in the presence of 2,3-dihydroxynaphthalene (2,3-DHN). $\pi-\pi$ stacking interactions between the naphthalene ring on the nanoplate surface are responsible for the formation of an ordered lamellar structure. 2,3-DHN molecules act not only as a stabilizer but also as a structure-directing agent. The nanoplates were successfully applied as a T1MRI contrast agent and showed a significant increase in relaxivity values, which can be attributed to their subnanometer thickness. Consequently, contrast enhancement of MR images was observed with a very low dose. The current synthetic process is easy to scale up to produce multigram quantities of the nanoplates. Furthermore, the synthetic approach can be generalized to fabricate other subnanometer thick nanoplates of transition metal oxides such as iron oxide and can be also used to produce ultrathin nanoplates that can be potentially applied to other areas such as energy storage and conversion, catalysis, and optoelectronics.

ASSOCIATED CONTENT

Supporting Information. TEM images and XRD pattern of manganese oxide nanoplates and iron oxide nanoplates, DLS, MTT assay data, and leaching test of water-dispersed manganese oxide nanoplates, *in vivo* MR images and intensity of the whole body, and confocal laser scanning microscopy image of the liver of a mouse model (PDF). This material is available free of charge via the Internet at http://pubs.acs.org.

AUTHOR INFORMATION

Corresponding Author
*E-mail: thyeon@snu.ac.kr.

ACKNOWLEDGMENT

We gratefully acknowledge the financial support by the Korean Ministry of Education, Science and Technology through National Creative Research Initiative (R16-2002-003-01001-0), Strategic Research (2010-0029138), and World Class University (R31-10013) Programs of National Research Foundation (NRF) of Korea.

REFERENCES

(1) Tang, Z.; Zhang, Z.; Wang, Y; Glotzer, S. C.; Kotov, N. A. *Science* **2006**, *314*, 274.
(2) Zhang, Q.; Ge, J.; Pham, T.; Goebl, J.; Hu, Y.; Lu, Z.; Yin, Y. *Angew. Chem., Int. Ed.* **2009**, *48*, 3516.
(3) Geim, A. K.; Novoselov, K. S. *Nat. Mater.* **2007**, *6*, 183.
(4) Pinna, N.; Niederberger, M. *Angew. Chem., Int. Ed.* **2008**, *47*, 5292.
(5) Oaki, Y.; Imai, H. *Angew. Chem., Int. Ed.* **2007**, *46*, 4951.
(6) Soejima, T.; Kimizuka, N. *J. Am. Chem. Soc.* **2009**, *131*, 14407.
(7) Liu, X.; Ma, R.; Bando, Y.; Sasaki, T. *Angew. Chem., Int. Ed.* **2010**, *49*, 8253.
(8) Kai, K.; Yoshida, Y.; Kageyama, H.; Saito, G.; Ishigaki, T.; Furukawa, Y.; Kawamata, J. *J. Am. Chem. Soc.* **2008**, *130*, 15938.
(9) Omomo, Y.; Sasaki, T.; Wang, L.; Watanabe, M. *J. Am. Chem. Soc.* **2003**, *125*, 3568.
(10) Puntes, V. F.; Zanchet, D.; Erdonmez, C. K.; Alivisatos, A. P. *J. Am. Chem. Soc.* **2002**, *124*, 12874.
(11) Wang, Y.; Hu, Y.; Zhang, Q.; Ge, J.; Lu, Z.; Hou, Y.; Yin, Y. *Inorg. Chem.* **2010**, *49*, 6601.
(12) Wang, C.; Hu, Y.; Lieber, C. M.; Sun, S. *J. Am. Chem. Soc.* **2008**, *130*, 8092.
(13) Srivastava, S.; Santos, A.; Critchley, K.; Kim, K.-S.; Podsiadlo, P.; Sun, K.; Lee, J.; Xu, C.; Lilly, G. D.; Glotzer, S. C.; Kotov, N. A. *Science* **2010**, *327*, 1355.
(14) Sigman, M. B., Jr.; Ghezelbash, A.; Hanrath, T.; Saunders, A. E.; Lee, F.; Korgel, B. A. *J. Am. Chem. Soc.* **2003**, *125*, 16050.
(15) Son, J. S.; Wen, X. D.; Joo, J.; Chae, J.; Baek, S.-I.; Park, K.; Kim, J. H.; An, K.; Yu, J. H.; Kwon, S. G.; Choi, S.-H.; Wang, Z.; Kim, Y.-W.; Kuk, Y.; Hoffmann, R.; Hyeon, T. *Angew. Chem., Int. Ed.* **2009**, *48*, 6861.
(16) Ithurria, S.; Dubertret., B. *J. Am. Chem. Soc.* **2008**, *130*, 16504.
(17) Yu, J. H.; Liu, X.; Kweon, K. E.; Joo, J.; Park, J.; Ko, K.-T.; Lee, D. W.; Shen, S.; Tivakornsasithorn, K.; Son, J. S.; Park, J.-H.; Kim, Y.-W.; Hwang, G. S.; Dobrowolska, M.; Furdyna, J. K.; Hyeon, T. *Nat. Mater.* **2010**, *9*, 47.
(18) Joo, J.; Son, J. S.; Kwon, S. G.; Yu, J. H.; Hyeon, T. *J. Am. Chem. Soc.* **2006**, *128*, 5632.
(19) Huo, Z.; Tsung, C.-K.; Huang, W.; Fardy, M.; Yan, R.; Zhang, X.; Li, Y.; Yang, P. *Nano Lett.* **2009**, *9*, 1260.
(20) Cao, Y. C. *J. Am. Chem. Soc.* **2004**, *126*, 7456.
(21) Xu, J.; Jang, K.; Jung, I. G.; Kim, H. J.; Oh, D.-H.; Ahn, D.-H.; Son, S. U. *Chem. Mater.* **2009**, *21*, 4347.
(22) Karmaoui, M.; Ferreira, R. A. S.; Mane, A. T.; Carlos, L. D.; Pinna, N. *Chem. Mater.* **2006**, *18*, 4493.
(23) Seo, J.-W.; Jun, Y.-W.; Park, S.-W.; Nah, H.; Moon, H.; Park, B.; Kim, J.-G.; Kim, Y. J.; Cheon, J. *Angew. Chem., Int. Ed.* **2007**, *46*, 8828.
(24) Yu, S.-H.; Yoshimura, M. *Adv. Mater.* **2002**, *14*, 296.
(25) Millstone, J. E.; Park, S.; Shuford, K. L.; Qin, L.; Schatz, G. C.; Mirkin, C. A. *J. Am. Chem. Soc.* **2005**, *127*, 5312.
(26) Jin, R.; Cao, Y. W.; Mirkin, C. A.; Kelly, K. L.; Schatz, K. L.; Zheng, K. L. *Science* **2001**, *294*, 1901.
(27) Krumeich, F.; Muhr, H.-J.; Niederberger, M.; Bieri, F.; Schnyder, B.; Nesper, R. *J. Am. Chem. Soc.* **1999**, *121*, 8324.
(28) Wang, C.; Hou, Y.; Kim, J.; Sun, S. *Angew. Chem., Int. Ed.* **2007**, *46*, 6333.
(29) Huo, Z.; Tsung, C.-k.; Huang, W.; Zhang, X.; Yang, P. *Nano Lett.* **2008**, *8*, 2041.
(30) Yin, Y.; Alivisatos, A. P. *Nature* **2005**, *437*, 664.

(31) Saunders, A. E.; Ghezelbash, A.; Sood, P.; Korgel, B. A. *Langmuir* **2008**, *24*, 9043.
(32) Murphy, C. J.; Sau, T. K.; Gole, A. M.; Orendorff, C. J.; Gao, J.; Gou, L.; Hunyadi, S. E.; Li, T. *J. Phys. Chem. B* **2005**, *109*, 13857.
(33) Xie, J.; Chen, K.; Lee, H.-Y.; Xu, C.; Hsu, A. R.; Peng, S.; Chen, X.; Sun, S. *J. Am. Chem. Soc.* **2008**, *130*, 7542.
(34) Lee, H.; Dellatore, S. M.; Miller, W. M.; Messersmith, P. B. *Science* **2007**, *318*, 426.
(35) Gu, H.; Xu, K.; Xu, C.; Xu, B. *Chem. Commun.* **2006**, 941.
(36) Yu, M.; Hwang, J.; Deming, T. J. *J. Am. Chem. Soc.* **1999**, *121*, 5825.
(37) Statz, A. R.; Meagher, R. J.; Barron, A. E.; Messersmith, P. B. *J. Am. Chem. Soc.* **2005**, *127*, 7972.
(38) Lee, H.; Lee, K. D.; Pyo, K. B.; Park, S. P.; Lee, H. *Langmuir* **2010**, *26*, 3790.
(39) Xu, C.; Xu, K.; Gu, H.; Zheng, R.; Liu, R.; Zhang, X.; Guo, X.; Xu, B. *J. Am. Chem. Soc.* **2004**, *126*, 9938.
(40) Kang, S. M.; Rho, J.; Choi, I. S.; Messersmith, P. B.; Lee, H. *J. Am. Chem. Soc.* **2009**, *131*, 13224.
(41) Grimme, S. *Angew. Chem., Int. Ed.* **2008**, *47*, 3430.
(42) Chen, O.; Zhuang, J.; Guzzetta, F.; Lynch, J.; Angerhofer, A.; Cao, Y. C. *J. Am. Chem. Soc.* **2009**, *131*, 12542.
(43) Yang, Z.; Liang, G.; Xu, B. *Acc. Chem. Res.* **2008**, *41*, 315.
(44) Mishra, A.; Behera, R. K.; Behera, P. K.; Mishra, B. K.; Behera, G. B. *Chem. Rev.* **2000**, *100*, 1973.
(45) Li, Y.; Wang, T.; Liu, M. *Tetrahedron* **2007**, *63*, 7468.
(46) Yam, V. W.-W.; Wong, K. M.-C.; Zhu, N. *J. Am. Chem. Soc.* **2002**, *124*, 6506.
(47) Song, C.; Ma, X.; Schmitz, A. D.; Schobert, H. H. *Appl. Catal., A* **1999**, *82*, 175.
(48) Farges, F. *Phys. Rev. B* **2005**, *71*, 155109.
(49) He, T.; Zhao, M.; Zhang, X.; Zhang, H.; Wang, Z.; Xi, Z.; Liu, X.; Yan, S.; Xia, Y.; Mei, L. *J. Phys. Chem. C* **2009**, *113*, 13610.
(50) Ma, R.; Liu, Z.; Li, L.; Iyi, N.; Sasaki, T. *J. Mater. Chem.* **2006**, *16*, 3809.
(51) Na, H. B.; Lee, J. H.; An, K.; Park, Y. I.; Park, M.; Lee, I. S.; Nam, D.-H.; Kim, S. T.; Kim, S.-H.; Kim, S.-W.; Lim, K.-H.; Kim, K.-S.; Kim, S.-O.; Hyeon, T. *Angew. Chem., Int. Ed.* **2007**, *46*, 5397.
(52) Bridot, J.-L.; Faure, A.-C.; Laurent, S.; Riviére, C.; Billotey, C.; Hiba, B.; Janier, M.; Josserand, V.; Coll, J.-L.; Elst, L. V.; Muller, R.; Roux, S.; Perriat, P.; Tillement, O. *J. Am. Chem. Soc.* **2007**, *129*, 5076.
(53) Shin, J.; Anisur, R. M.; Ko, M. K.; Im, G. H.; Lee, J. H.; Lee, I. S. *Angew. Chem., Int. Ed.* **2009**, *48*, 321.
(54) Taylor, K. M. L.; Rieter, W. J.; Lin, W. *J. Am. Chem. Soc.* **2008**, *130*, 14358.
(55) An, K.; Park, M.; Yu, J. H.; Na, H. B.; Lee, N.; Park, J.; Choi, S. H.; Song, I. C.; Moon, W. K.; Hyeon, T. Synthesis of uniform-sized manganese oxide nanocrystals with various sizes and shapes and investigation of their T1 magnetic resonance relaxivity, unpublished work.
(56) An, K.; Kwon, S. G.; Park, M.; Na, H. B.; Baik, S.-I.; Yu, J. H.; Kim, D.; Son, J. S.; Kim, Y. W.; Song, I. C.; Moon, W. K.; Park, H. M.; Hyeon, T. *Nano Lett.* **2008**, *8*, 4252.
(57) Huang, C.-C.; Khu, N.-H.; Yeh, C.-S. *Biomaterials* **2010**, *31*, 4073.
(58) Gilad, A. A.; Walczak, P.; McMahon, M. T.; Na, H. B.; Lee, J. H.; An, K.; Hyeon, T.; van Zijl, P. C. M.; Bulte, J. W. M. *Magn. Reson. Med.* **2008**, *60*, 1.
(59) Lauffer, R. E. *Chem. Rev.* **1987**, *87*, 901.
(60) Alexis, F.; Pridgen, E.; Molnar, L. K.; Farokhzad, O. C. *Mol. Pharmaceutics* **2008**, *5*, 505.
(61) Furumoto, K.; Ogawara, K.-I.; Yoshida, M.; Takakura, Y.; Hashida, M.; Higaki, K.; Kimura, T. *Biochim. Biophys. Acta* **2001**, *1526*, 221.
(62) Liu, Z.; Davis, C.; Cai, W.; He, L; Chen, X.; Dai, H. *Proc. Natl. Acad. Sci. U.S.A.* **2008**, *105*, 1410.